ADVANCED FUNCTIONAL MATERIALS
www.afm-journal.de

Development of Therapeutic Small-Molecule Fluorophore for Cell Transplantation

*Xin Wang, Zelin Chen, Shenglin Luo, Taotao Jin, Yu Wang, Fuqin Chen, Liao Wu, Xu Tan, and Chunmeng Shi**

Cell transplantation holds great promise in regenerative medicine but restricted cell survival and tracking severely limited their therapeutic efficacy. The development of multifunctional agents to simultaneously address these challenges will be very helpful in cytotherapy. Near-infrared (NIR) imaging is being increasingly used for in vivo cell tracking, but the extensive cell contamination and potential cytotoxicity of current membrane lipophilic dyes severely limit their potentialuse in clinical applications. Here, a novel mitochondrial heptamethine dye, NIR cell protector-61 (NIRCP-61), is designed and synthesized via modification of *N*-alkyl side chains around a heptamethine core, which maintains the superior fluorescent imaging properties and significantly decreases cell contamination. Further, NIRCP-61 also significantly alleviates cell damage from acute oxidative stress and improves their therapeutic outcome in multiple animal models. This cytoprotective effect is mediated by evoking the intracellular antioxidant defense mechanisms of nuclear factor erythroid 2-related factor 2 (Nrf2) and phosphoinositide 3-kinase/protein kinase B (PI3K/Akt) pathways. NIRCP-61 is the first NIR agent that simultaneously meets the requirements for both cell tracking and cytoprotection. Therefore, NIRCP-61 may represent an attractive therapeutic fluorophore for cell transplantation and offers a convenient way to impel potential translation in clinical cell-based therapies.

1. Introduction

Cell transplantation has recently initiated increasing interests in regenerative medicine,[1] but the very restricted cell survival and tracking at wounded sites after transplantation significantly limited their potential in clinical application.[2] Thus, there is an urgent need to develop multifunctional agents for cytotherapy by implementing the cytoprotective activity and cell tracking ability simultaneously. To our knowledge, there are no such agents that have been reported so far. Near-infrared (NIR) imaging possesses great potential for noninvasive in vivo imaging due to low tissue auto-fluorescence and deeper tissue penetration,[3] which is currently available in biomedical imaging.[4] Heptamethine cyanine dyes are representative NIR fluorescent agents and a couple of these dyes have been extensively used for in vivo cell labeling and tracking.[5] Of them, the indocyanine green (ICG), which is approved for clinical use as diagnostic reagent for a few decades, is recently emerging as a potential NIR agent in clinic for cell labeling and tracking. However, most organic dyes are membrane lipophilic and the extensive cell contamination and potential cytotoxicity of these dyes severely hurdle their potential in clinical application.[6] The development of an agent with both cell tracking and cytoprotective activities will be very helpful in cell-based therapy.

In our recent work, we have identified a class of lipophilic NIR fluorescent heptamethine cyanine dyes, which are able to preferentially accumulate into cell mitochondria[7,8] and possess unique optical properties for in vivo cell tracking and biomedical imaging.[9] Our structure–activity relationship study[10] and other reports[11] have indicated that the heptamethine core with lipophilic cationic property is essential for mitochondrial targeting. Based on these foregoing studies, in this work, we designed and synthesized a series of heptamethine dyes modified with various *N*-alkyl side chains around the heptamethine core, and successfully developed a new derivative, termed NIR cell protector-61 (NIRCP-61), which maintains the superior optical imaging properties and significantly decreases the cell contamination. More importantly, as a mitochondrial agent, NIRCP-61 significantly alleviates the cell damage caused by acute oxidative stress after transplantation and improves their therapeutic outcome in multiple animal models. This cytoprotective effect is mediated by evoking the intracellular antioxidant defense mechanisms of Nrf2 and phosphoinositide 3-kinase/protein kinase B (PI3K/Akt) pathways, consequently

Dr. X. Wang, Dr. Z. Chen, Dr. S. Luo, T. Jin, Dr. Y. Wang, L. Wu, X. Tan, Prof. C. Shi
Institute of Combined Injury
State Key Laboratory of Trauma
Burns and Combined Injury
Chongqing Engineering Research
Center for Nanomedicine
College of Preventive Medicine
Third Military Medical University
30th Gaotanyan street, Chongqing 400038, China
E-mail: shicm@sina.com
F. Chen
School of Public Health
Gui Zhou Medical University
Guiyang 550004, China

DOI: 10.1002/adfm.201600996

increasing the cell survival and improving the therapeutic potential. Therefore, NIRCP-61 may represent an attractive therapeutic fluorophore for cell transplantation and offers a convenient way to impel potential clinical translation in cell-based therapies.

2. Results

2.1. Synthesis and Optical Properties of NIRCP-61

As shown in **Figure 1**a, synthesis of NIRCP-61 was started with cyclohexanone (compound **1**) and 2,2,3-trimethyl-3H-indolenine (compound **3**) as the initial materials and was finally completed with a condensation reaction between compounds **2** and **4**. Compound **2** was synthesized according to our previously reported protocol.[7] Indolenine quaternary ammonium salt (compound **4**) was synthesized by following method and it was afforded and straightforward used in the next reaction without further purification: 2,2,3-trimethyl-3H-indolenine (30×10^{-3} M) and 4-bromomethyl-benzoic acid (30×10^{-3} M) were mixed in 1,2-dichlorobenzene (15 mL) and stirred at 110 °C under argon protection for 12 h. The reaction mixture was cooled to room temperature and added to acetone. The brown precipitate was collected and washed with acetone. Subsequently, Compound **4** (7×10^{-3} M) was reacted with compound **2** (3.5×10^{-3} M) by a condensation reaction in a 30 mL of absolute ethanol solution of sodium acetate (3.5×10^{-3} M) to finally synthesize NIRCP-61 (308.7 mg, green powder, yield 11%, melting point: 202–208 °C). The chemical structure of NIRCP-61 was characterized using ^{1}H and ^{13}C nuclear magnetic resonance (NMR) and high-resolution mass spectrometry (HRMS). ^{1}H NMR (400 Hz, dimethyl sulfoxide (DMSO)-d_6) δ: 8.26 (d, J = 14.4 Hz, 2H), 7.94 (d, J = 8.0 Hz, 4H), 7.69 (d, J = 7.6 Hz, 2H), 7.40 (t, J = 7.2 Hz, 8H), 7.33–7.28 (m, 2H), 6.38 (d, J = 14.0 Hz, 2H), 5.63 (s, 4H), 2.53–2.50 (m, 4H), 1.73 (s, 14H); ^{13}C NMR (100 MHz, DMSO-d_6) δ: 172.901, 167.239, 148.461, 143.525, 142.331, 140.939, 129.925, 129.664, 129.502, 128.749, 127.023, 126.575, 125.393, 111.638, 102.334, 99.592, 49.160, 48.591, 46.979, 45.218, 27.858, 27.604, 25.700, 19.904;

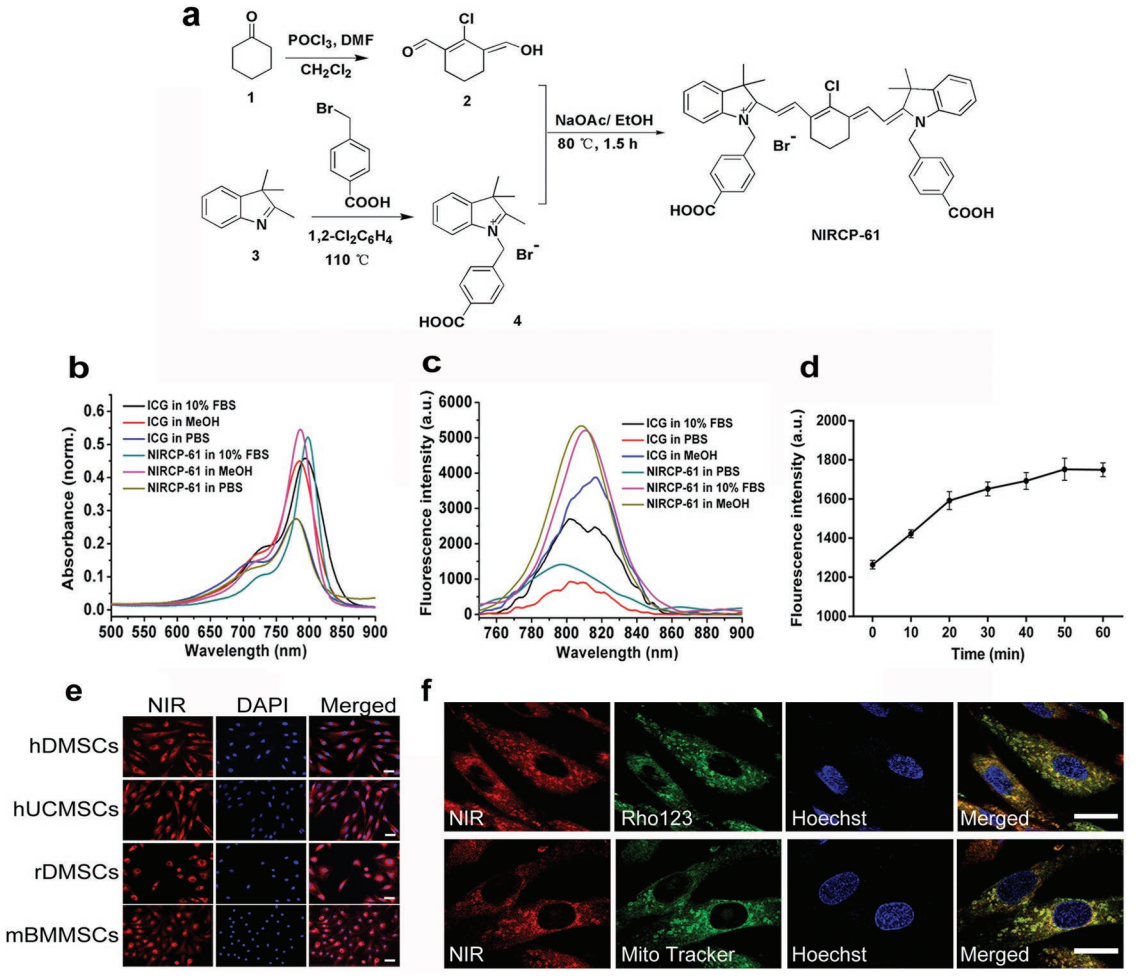

Figure 1. Chemical synthesis, optical properties, and subcellular localization of NIRCP-61. a) Synthetic route and chemical structure of NIRCP-61. b) NIR absorption spectra and c) NIR emission spectra of 2×10^{-6} M NIRCP-61 and ICG in methanol, PBS, and 10% FBS, respectively. d) Fluorescence stability of 2×10^{-6} M NIRCP-61 in 10% FBS at 37 °C for 60 min. e) Four types of primary MSCs were labeled indistinguishably by NIRCP-61 in vitro. 4,6 Diamidino-2-phenylindole (DAPI) was used to stain cell nuclei. f) NIRCP-61-labeled hUCMSCs were costained with rhodamine 123 and Mito-Tracker Green, and subcellular localization of NIRCP-61 was imaged by confocal microscopy. Hoechst 33342 was used to stain nuclei. Bars represent 100 μm (e) and 20 μm (f).

Adv. Funct. Mater. 2016,
DOI: 10.1002/adfm.201600996

HRMS [M-Br]$^+$: calc. 723.2984, measured 723.2882. According to the absorption and fluorescence spectra of NIRCP-61 that was investigated in methanol (MeOH), 10% fetal bovine serum (FBS) and phosphate-buffered saline (PBS), the absorption and emission peak of NIRCP-61 was in the NIR region (Figure 1b,c). Its optical properties, including the maximal absorbance and emission peak, molar absorption coefficient, stokes shift and relative fluorescence quantum yield were calculated, as shown in Table S1 (Supporting Information). The fluorescent intensity of NIRCP-61 in MeOH, 10% FBS, and PBS was higher than that of ICG. Photostability of NIRCP-61 in 10% FBS at 37 °C (Figure 1d) revealed that the total fluorescence emission of NIRCP-61 increased within the first 30 min and then gradually reached a stable level, suggesting good potential for biomedical imaging.

2.2. In Vitro Cell Preconditioning, Biocompatibility, and Subcellular Localization of NIRCP-61

To confirm the optimal labeling procedure, mesenchymal stem cells (MSCs) derived from human umbilical cord (hUCMSCs) and human dermis (hDMSCs) were preconditioned with NIRCP-61 at various incubation times and concentrations. Cell imaging revealed that NIRCP-61 uptake was time and concentration dependent and approached a plateau after 30 min or 20×10^{-6} M incubation (Figure S1, Supporting Information). Based on these findings, incubation with 20×10^{-6} M NIRCP-61 for 30 min was expected to achieve optimal labeling fluorescence. Biocompatibility assessment showed that incubating alone under such incubation condition achieved the successful labeling of all cells without the application of additional transfection agents and/or procedures; meanwhile, it did not show cytotoxicity on the physiology of labeled cells (Figure S2, Supporting Information). We further labeled MSCs derived from different organs and species, including mouse bone marrow MSCs (mBMMSCs), rat dermis MSCs (rDMSCs), hUCMSCs, and hDMSCs to confirm the labeling capability of NIRCP-61 and found that the MSCs used in this experiment were effectively labeled without obvious differences in fluorescence (Figure 1e). Considering that hUCMSCs are commonly used in current clinical therapy, we focused on hUCMSCs to conduct further studies, except where explicitly stated. Moreover, cell imaging detected on days 0, 1, 2, 3, and 6 after labeling revealed that although the fluorescent intensity gradually decreased in a time-dependent manner, it was still detectable on day 6, indicating superior in vitro fluorescence stability (Figure S3, Supporting Information). Furthermore, costaining with the mitochondria-specific fluorescence probes rhodamine 123 and Mito-Tracker Green (Beyotime), visualization of subcellular localization confirmed that NIRCP-61 was distributed particularly in the cell mitochondria (Figure 1f).

2.3. Dye Transfer and Specific Fluorescence Signaling of Labeled MSCs

Massive dye transfer to neighboring cells was observed by current membrane lipophilic dyes both in vitro and in vivo.[6] Because of localization to the mitochondria, we hypothesized that NIRCP-61 labeling could decrease dye contamination; thus, dye transfer of NIRCP-61 was assessed and compared with a widely used membrane lipophilic dye, 1,1′-dioctadecyl-3,3,3′,3′-tetramethylindotricarbocyanine perchlorate (DiI) as control. After coculturing with hDMSCs expressing enhanced green fluorescent protein (eGFP), NIRCP-61 labeling revealed a much less dye transfer than DiI, as affirmed by live confocal imaging (**Figure 2**a) and flow cytometry (Figure 2b,c). Quantification of fluorescence associated with NIRCP-61-labeled hUCMSCs was significantly higher than that with DiI-labeled hUCMSCs (Figure 2d). We then investigated the feasibility of in vivo cell imaging and tracking for NIRCP-61. Mice with dorsal trauma combined with radiation were systemically intravenously administered NIRCP-61-labeled eGFP$^+$mBMMSCs. Cell migration and homing to distant injury sites were imaged using the Kodak In-Vivo FX Professional Imaging System. At 10 min after transplantation, the lung and liver were visualized for the whole animal imaging, especially in the real-time intraoperative images of animals with opening abdominal walls and thoracic cavity, and the imaging of dissected organs showed that the infused MSCs were distributed in lung, liver, heart, and kidney. After 24 h, whole animal imaging and ex vivo assessments revealed that the NIR signal was from the wound tissues (Figure 2e, left panels), indicating that transplanted MSCs had migrated to dorsal injury sites. Colocalization of NIR fluorescence and eGFP signal in the tissues further confirmed that the NIR fluorescence detected was exactly derived from transplanted eGFP$^+$mBMMSCs (Figure 2f). To further verify this finding, we smashed labeled eGFP$^+$mBMMSCs with an ultrasonic disruptor and infused the cell debris in mouse model. At the same time point postinjection, fluorescence signal was detected primarily in liver, and no NIR fluorescenece was detected in wound tissues (Figure 2e, right panels). These data revealed that NIRCP-61 demonstrated excellent properties of cell labeling for cell imaging and tracking in vivo.

2.4. NIRCP-61 Protects MSCs from Oxidative Stress

A growth curve assay revealed that the proliferation of NIRCP-61-preconditioned MSCs had slightly increased after 3 d (Figure S4a, Supporting Information). We proposed that NIRCP-61 might increase the resistance of cells to adverse factors, such as oxidative stress. So, we used hydrogen peroxide (H_2O_2) and ionizing radiation (IR) to mimic cell damage caused by oxidative stress in vitro. MSCs preconditioned with NIRCP-61 demonstrated better resistance to acute oxidative stress induced by H_2O_2 with less cell damage and apoptosis (**Figure 3**a,b). To visually evaluate cell survival after H_2O_2 treatment, MSCs were costained with calcein-AM (Invitrogen) and propidium iodide (PI) to estimate live and dead/late apoptotic cells, respectively. As shown in Figure 3c, all normal and NIRCP-61-labeled MSCs displayed green fluorescence, indicating that NIRCP-61 does not induce cell death, but H_2O_2 treatment induced severe cell death (red fluorescence), whereas NIRCP-61 dramatically reversed this effect. Moreover, clonogenic survival assays also revealed a significant increase in the survival of NIRCP-61-labeled MSCs post-IR compared with normal cells (Figure 3d,e).

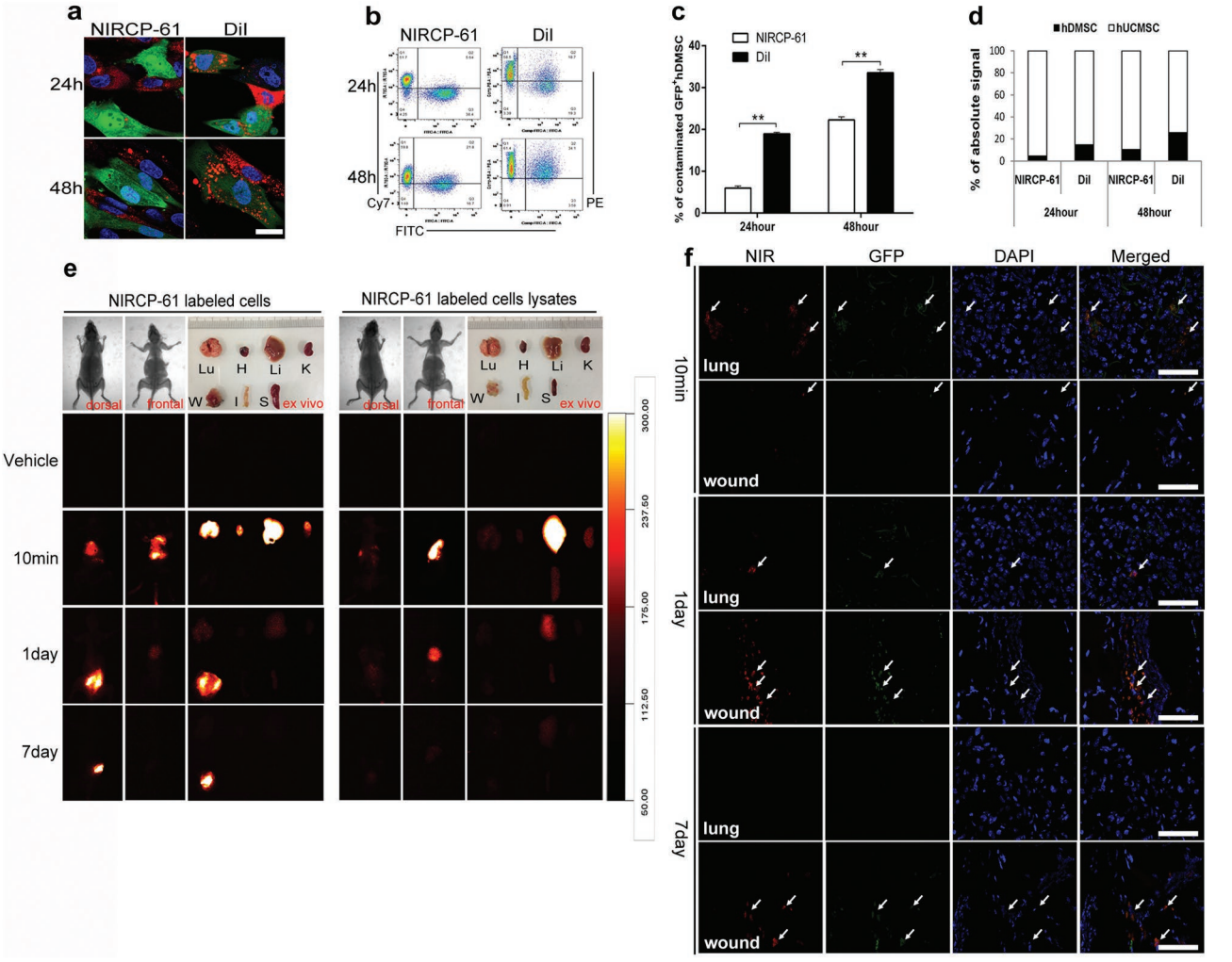

Figure 2. NIRCP-61 allows whole-body imaging and tracking of MSCs with limited dye transfer to neighboring cells. NIRCP-61- or DiI-labeled hUCMSCs were cocultured with eGFP$^+$hDMSCs for 24 or 48 h. After coculturing, dye transfer was analyzed by confocal imaging a) and flow cytometry b–d). a) After 24 or 48 h of coculture, dye (red fluorescence) transfer to eGFP$^+$hDMSCs (green fluorescence) was detected by confocal microscopy. Nuclei were stained with Hoechst 33342 (blue fluorescence). b,c) After 24 or 48 h of coculture, the percentage of eGFP$^+$hDMSCs (fluorescein isothiocyanate, FITC) contaminated by NIRCP-61 (cyanine 7, Cy7) was 5.99% ± 0.50% and 18.95% ± 0.35%, while the percentage of cells contaminated by DiI (phycoerythrin, PE) was 22.3% ± 0.71% and 33.6% ± 0.78% ($P < 0.01$), respectively. d) Absolute quantification of fluorescence (expressed as percentage of total fluorescence) associated with NIRCP-61-labeled cells was 95.64% ± 0.003% and 89.69% ± 0.005%, and that of DiI-labeled cells was 85.19% ± 0.003% and 74.21% ± 0.018% ($P < 0.01$), respectively. e) In vivo (dorsal and frontal acquisition) and ex vivo NIR fluorescence images of mice at indicated time after systemic administration of NIRCP-61-labeled eGFP$^+$mBMMSCs (2×10^6 cells, left panels) or NIRCP-61-labeled eGFP$^+$mBMMSCs lysates (right panels) by intravenous injection. The frontal acquisition was performed with opening abdominal walls and thoracic cavity. f) Confocal images of NIRCP-61-labeled eGFP$^+$mBMMSCs (white arrows) in different tissues at indicated time. Lu, lung; H, heart; Li, liver; K, kidney; W, wound tissues; I, intestine; S, spleen. Bars represent 20 μm (a) and 50 μm (f).

Abundant reactive oxygen species (ROS) is generated and maintained at a high level in cells following IR or H_2O_2 treatment, causing severe DNA double strand breaks (DSBs) and induce apoptosis.[12] We treated MSCs with IR and H_2O_2 to determine whether NIRCP-61 alleviates cell death by reducing ROS accumulation. Results showed that NIRCP-61 caused a reduction in ROS level after IR or H_2O_2 treatment (Figure S4b,c, Supporting Information), suggesting that attenuated ROS damage may contribute to cytoprotection. To test this possibility, γ-H2AX was subsequently assessed as a DNA DSBs response marker. Results showed that NIRCP-61 significantly reduced γ-H2AX formation post-IR compared with normal cells (Figure 3f–i). Furthermore, results of comet assay showed that NIRCP-61 significantly decreased tail length, tail DNA%, and olive tail moment compared to control cells (Figure 3j–m). These results supported that NIRCP-61 could decrease ROS accumulation and alleviate the DNA DSBs.

2.5. NIRCP-61 Enhances Antioxidant Ability via Modulation of the Nrf2 and PI3K/Akt Pathways

In prior studies, we found that NIRCP-61 attenuated ROS accumulation after IR or H_2O_2 treatment. Therefore, mitochondrial

DOI: 10.1002/adfm.201600996

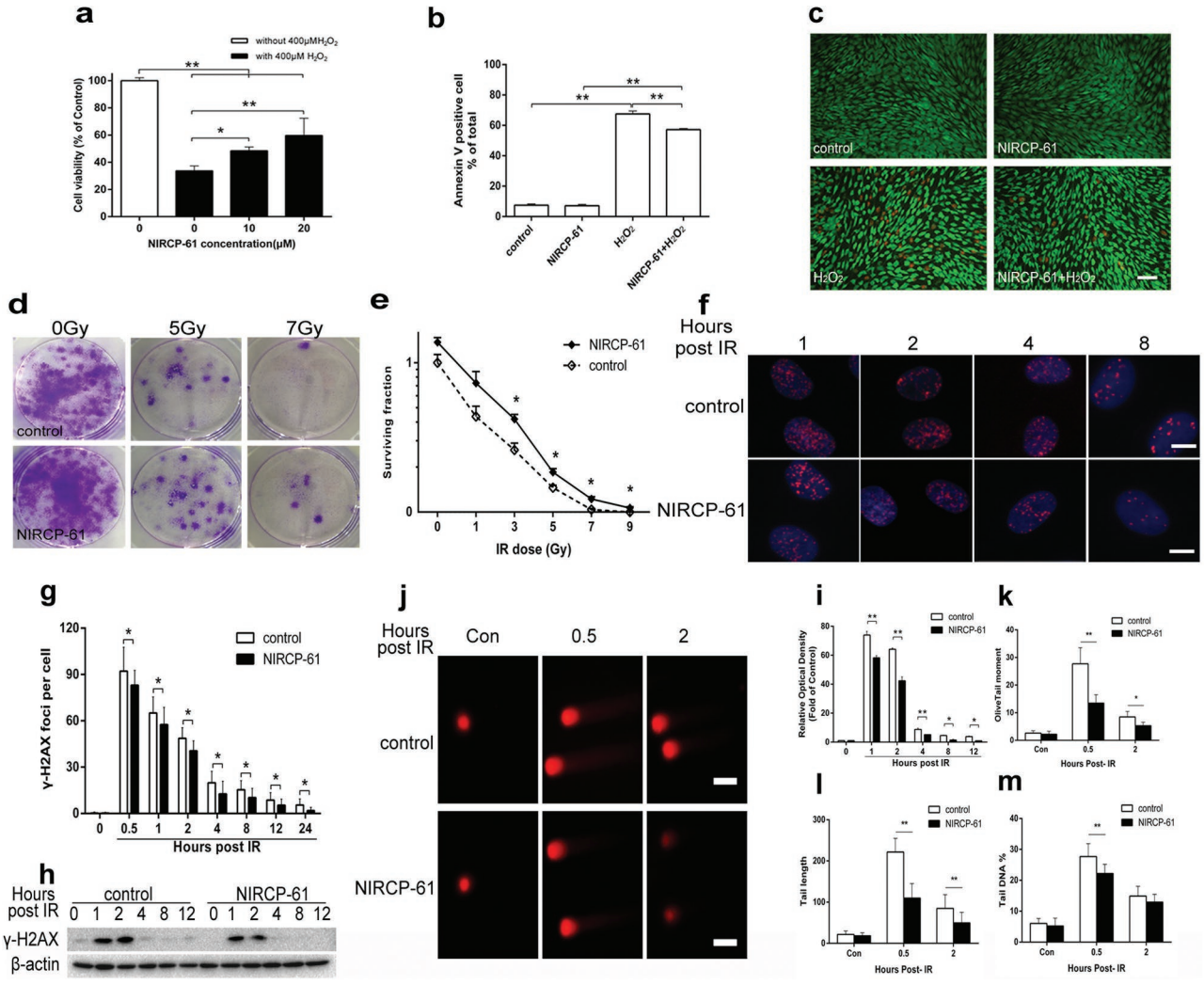

Figure 3. NIRCP-61 increases cell survival and alleviates DNA DSBs induced by oxidative stress. a) H_2O_2 treatment significantly decreased cell viability, while NIRCP-61 reversed this decrease dramatically (*, $P < 0.05$; **, $P < 0.01$). b) NIRCP-61 significantly decreased apoptosis induced by H_2O_2 treatment ($P < 0.01$). c) Cells were costained with calcein-AM and PI to visualize live cells (green fluorescence) and dead/late apoptotic cells (red fluorescence) after H_2O_2 treatment, respectively. NIRCP-61 obviously decreased H_2O_2-induced cell death. Clonogenic survival assay showed that NIRCP-61 enhanced MSCs survival post-IR. d) Representative images of hUCMSCs colonies generated in survival assays following 0/5/7 Gy IR. e) Fraction of hUCMSCs surviving after IR ($P < 0.05$). f) Representative images of nuclei γ-H2AX in hUCMSCs 1–8 h post-IR. g) Average number of γ-H2AX per nucleus 0–24 h post-IR ($P < 0.05$). h,i) Representative blots and quantification of Western blot analysis of γ-H2AX expression in hUCMSCs post-IR (*, $P < 0.05$; **, $P < 0.01$). j) Representative nucleolus images of comet assay post-IR. k–m) Average olive tail moment, tail length, and tail DNA% per nucleus post-IR (*, $P < 0.05$; **, $P < 0.01$). Con, control. Bars represent 100 μm (c), 20 μm (f), and 50 μm (j).

and cytosolic superoxide variations were further assessed to determine whether NIRCP-61 directly decreased intracellular ROS generation. The MitoSOX red and 2′,7′-dichlorofluorescin diacetate (H_2DCF-DA) assay revealed that NIRCP-61 provoked a transient release of mitochondrial and cytosolic superoxide, but the elevated ROS levels quickly reverted to normal levels and the cytosolic ROS levels of NIRCP-61-preconditioned cells were even lower than that of nonpreconditioned control cells after 24 h (**Figure 4**a,b). Thus, we supposed that the protective effect of NIRCP-61 was mediated by an increased intracellular ROS scavenging capacity. We measured the levels of different antioxidants involved in ROS scavenging and found that superoxide dismutase (SOD2, SOD1), glutathione peroxidase-1 (GPX-1), and catalase (CAT) expression levels were increased after NIRCP-61 preconditioning (Figure 4c and Figure S5a, Supporting Information).

Previous reports indicated that short-term exposure to low doses of oxidative stress could increase cell survival and improve cell function.[13] Similar to oxidative stress exposure, NIRCP-61 mildly increased intracellular ROS level, which could accelerate Nrf2 separating from Kelch-like epichlorohydrin-associated protein 1 (Keap1) and transporting into the nucleus where it combined with antioxidant response elements. Furthermore, elevated intracellular ROS level activates the PI3K/Akt pathway, which subsequently phosphorylates Nrf2 and glycogen synthase kinase-3β (GSK-3β),[14] a negative modulator of Nrf2.[15] To test this hypothesis, we assessed proteins relevant to the Nrf2 and PI3K/Akt pathways. As shown in Figure 4d and

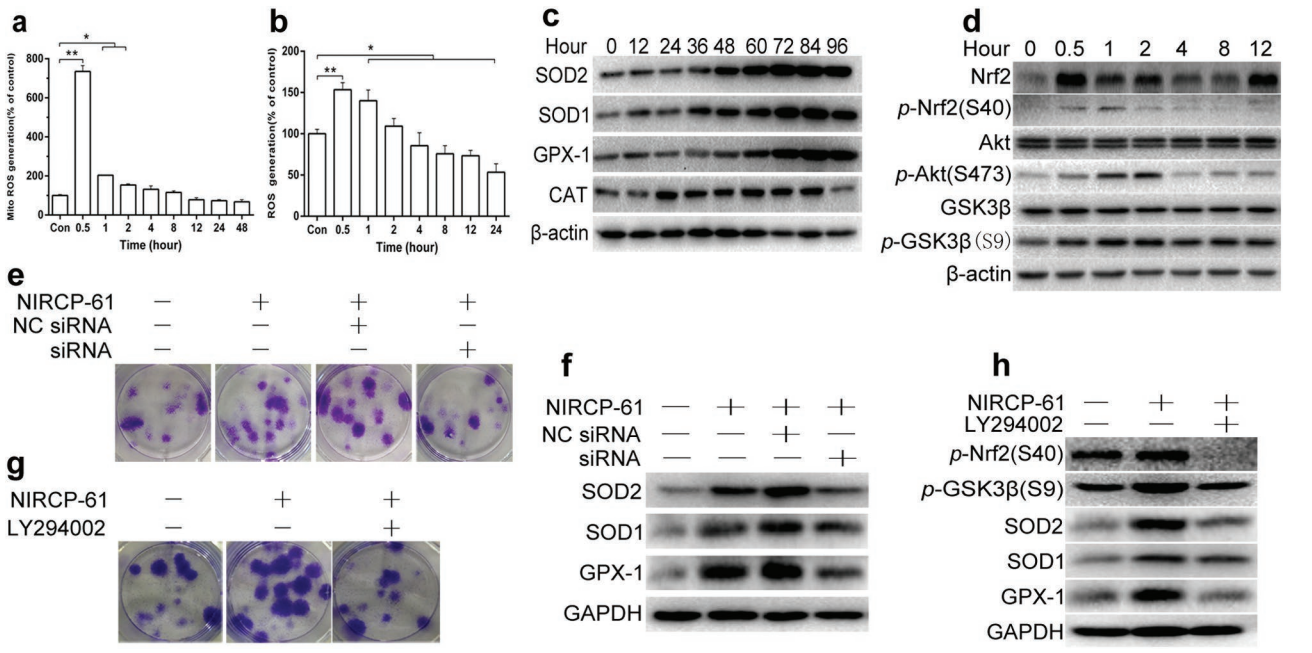

Figure 4. NIRCP-61 promotes antioxidant defense of MSCs via modulation of Nrf2 and PI3K/Akt pathways. a) Mitochondrial superoxide variation at 0–48 h after NIRCP-61 preconditioning (*, $P < 0.05$; **, $P < 0.01$). b) Intracellular ROS variation at 0–24 h after NIRCP-61 preconditioning (*, $P < 0.05$; **, $P < 0.01$). c) SOD2, SOD1, GPX-1, and CAT expression levels in whole cell lysates from NIRCP-61-preconditioned hUCMSCs for the indicated times. d) Nrf2, *p*-Nrf2, Akt, *p*-Akt, GSK-3β, and *p*-GSK-3β expression levels in whole cell lysates from NIRCP-61-preconditioned hUCMSCs for the indicated times. e) Representative images of hUCMSCs colonies generated in clonogenic survival assays following IR. f) SOD2, SOD1, and GPX-1 expression levels in whole cell lysates from NIRCP-61-preconditioned hUCMSCs transfected with or without Nrf2 siRNA for 72 h. g) Representative images of hUCMSCs colonies generated in survival assays following IR. h) *p*-Nrf2, *p*-GSK-3β, SOD2, SOD1, and GPX-1 expression levels in whole cell lysates from NIRCP-61-preconditioned hUCMSCs cultured with or without LY294002 (40×10^{-6} M) for 72 h. Con, control.

Figure S5b (Supporting Information), NIRCP-61 increased Nrf2 expression and promoted phosphorylation of Nrf2, Akt, and GSK-3β. Small interfering RNA (siRNA) oligo against Nrf2 and PI3K/Akt inhibitor LY294002 were used to explore the possible involvement of the Nrf2 and PI3K/Akt pathways in mediating cell survival. Incubation with either Nrf2 siRNA or the PI3K/Akt inhibitor LY294002 both significantly reduced the clonogenic capacity of NIRCP-61-preconditioned MSCs after IR and decreased intracellular antioxidants expression (Figure 4e–h and Figure S5c,d, Supporting Information). These results indicate that NIRCP-61 activates Nrf2 and PI3K/Akt pathways and induces intracellular antioxidative defense.

2.6. NIRCP-61 Improves Survival and Therapeutic Effects of Transplanted MSCs in Multiple In Vivo Models

Considering the cell protective effects of NIRCP-61 in vitro, we next explored if NIRCP-61 could rescue MSCs from the noxious effects of oxidative stress in vivo. Myocardial infarction (MI) is considered as a microenvironment with severe oxidative stress. Therefore, we tested whether NIRCP-61 could increase transplanted cell survival and improve therapeutic effects. Results exhibited that the left ventricle (LV) infarct size was significantly smaller in rats infused with NIRCP-61-preconditioned hUCMSCs than those with hUCMSCs or vehicle at 4 weeks post-MI (**Figure 5**a,b). MI significantly decreased LV fractional shortening and ejection fraction in vehicle- and hUCMSCs-treated rats, while heart function was obviously maintained by NIRCP-61-preconditioned hUCMSCs transplantation (Figure 5c–f). Moreover, the transplantion of NIRCP-61-preconditioned hUCMSCs significantly decreased the enlargement of diastolic left ventricle internal diameter caused by MI at 4 weeks (Figure 5g). Survival of transplanted eGFP$^+$hUCMSCs and Masson's trichrome staining demonstrated that NIRCP-61 increased cell retention and survival and reduced fibrotic areas of the peri-infarct regions at 4 weeks post-MI (Figure 5h–k). In addition, it is well known that radiation delays wound healing, which remains a clinical challenge. Thus, we further tested the therapeutic effects of NIRCP-61 on transplanted hUCMSCs in a combined IR and wound injury rat model. Wound healing was faster in rats treated with NIRCP-61-preconditioned hUCMSCs than in those treated with the vehicle or hUCMSCs, particularly at days 3 and 5 (**Figure 6**a). Scar thickness was significantly thinner in rats transplanted with NIRCP-61-preconditioned hUCMSCs than in other groups (Figure 6b,c). Much more eGFP$^+$ cells were found in the wound tissue of rats treated with NIRCP-61-preconditioned eGFP$^+$hUCMSCs compared with those treated with eGFP$^+$hUCMSCs (Figure 6d,e). Furthermore, we administrated NIRCP-61-preconditioned hUCMSCs to a much more challenging rat model of one hindlimb receiving a high radiation dose (40 Gy) exposure, resulting in erythema aggravation, desquamation, and skin ulceration. The results showed that NIRCP-61-preconditioned hUCMSCs significantly decreased formation of IR-induced cutaneous ulceration and edema and increased dermal cell restoration and

DOI: 10.1002/adfm.201600996

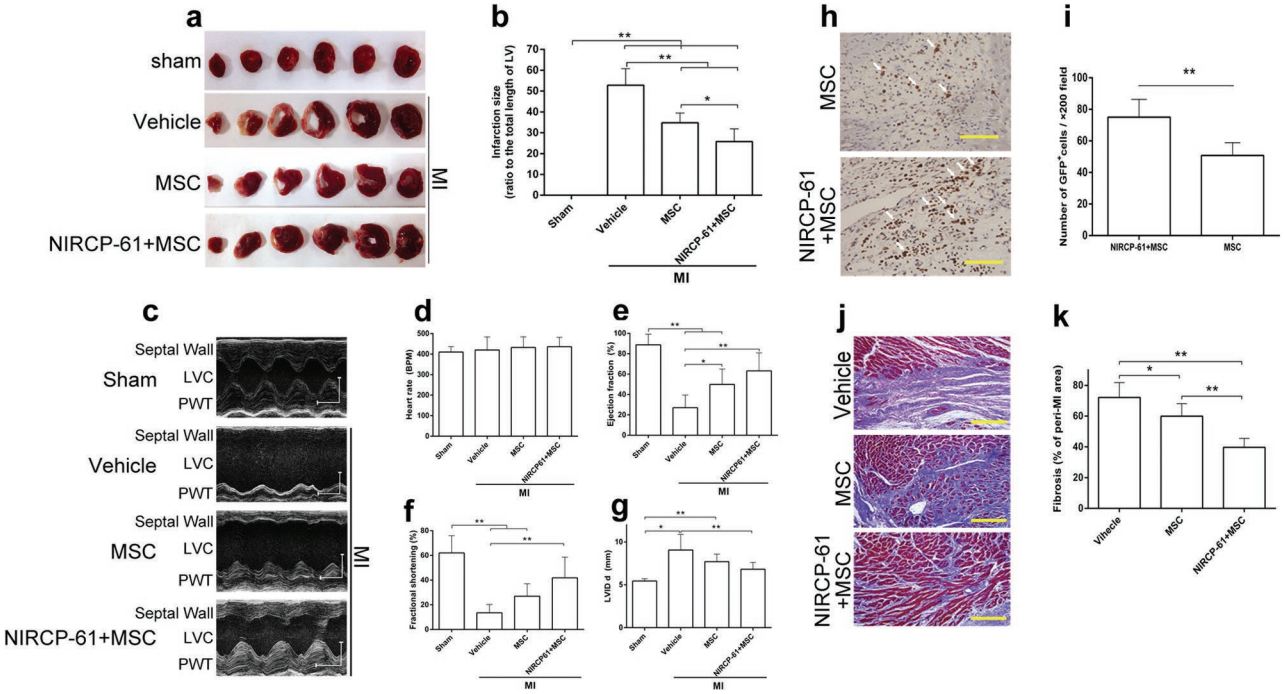

Figure 5. Transplantation of NIRCP-61-preconditioned MSCs reduces infarct size and improves cardiac function in MI rats. a) Representative images of heart sections (triphenyl tetrazolium chloride stained) of rats from different groups 4 weeks after MSCs transplantation. b) The percentage of infarction size (expressed as the ratio of the length of the infarct region to the total length of left ventricle; *, $P < 0.05$; **, $P < 0.01$; $n = 7$). c) Representative M-mode images of hearts from rats of different groups 4 weeks after MSCs transplantation. Scale bar, x-axis represents 0.1 s; y-axis represents 0.3 cm. d) Heart rates were similar among different groups. e–g) LV ejection fraction, fractional shortening, and diastolic left ventricle internal diameter (LVIDd) at 4 weeks after MSCs transplantation (*, $P < 0.05$; **, $P < 0.01$; $n = 7$). h,i) Representative images and quantification of surviving NIRCP-61-preconditioned eGFP$^+$hUCMSCs in infarcted regions of the heart (white arrows) were detected on day 7 posttransplantation. Transplanted eGFP$^+$hUCMSCs survived in infarcted regions of the heart, and NIRCP-61 significantly increased cell retention and survival in infarcted areas ($P < 0.01$; $n = 3$). j) Representative images of fibrotic regions in peri-infarct areas by Masson's trichrome staining at 4 weeks after MI. k) Quantification of fibrotic areas in peri-infarct regions indicates that fibrosis was significantly reduced by MSCs treatment, and NIRCP-61-preconditioned MSCs further reduced it (*, $P < 0.05$; **, $P < 0.01$; $n = 3$). Bars represent 200 µm (h,j).

reepithelialization two weeks after IR (Figure 6f). Altogether, these data suggest that NIRCP-61 could increase the retention and survival of transplanted MSCs and improve functional effects of transplanted MSCs in vivo. In order to evaluate the in vivo toxicity of NIRCP-61, histological examination of vital organs (including heart, lung, liver, spleen, kidney, and brain) was performed on day 7 after cell transplantation and there was no pathological alterations observed in mice receiving NIRCP-61-preconditioned mBMMSCs as compared to control mice (Figure S6, Supporting Information). We also injected a fivefold dose of the preconditioning dose through tail vein to observe the acute toxicity of NIRCP-61 in mice. The results of blood routine, renal/liver function parameters, and hematoxylin and eosin (H&E) staining images of vital organs showed that there was no abnormal changes in NIRCP-61 treated mice as compared to control mice (Tables S2 and S3, and Figure S7, Supporting Information), further supporting the promise of NIRCP-61 as a potential agent for cell transplantation.

3. Discussion

Cell therapy is a promising strategy for treating various diseases which have limited regenerative capacity, such as neurodegenerative disease, cardiovascular disease, and radiation injury.[16] However, restricted cell survival in diseased sites and poor understanding of cell fate after transplantation are major hurdles currently limiting the clinical translation of cell therapies.[2] Therefore, it is very urgent to develop multifunctional agents to simultaneously overcome these two obstacles. NIR imaging following cell transplantation enables estimating cellular behavior in vivo, understanding critical cellular mechanisms and cell functional contributions to regeneration.[17] However, the current NIR membrane lipophilic dyes are not ideal agents for cell tracking because of massive contamination and potential cytotoxicity. In this study, we designed and synthesized a novel mitochondrial heptamethine dye, NIRCP-61, through chemical structural modification, which maintains the NIR fluorescence properties for cell labeling and tracking in vivo with significantly decreased contamination to proximal cells. More remarkably, we identified NIRCP-61 as a novel agent to improve survival and physiological functions of engrafted cells against oxidative stress and achieve a preferable therapeutic effect in multiple animal models.

Sufficient evidence indicates that oxidative stress caused by ischemia/reperfusion injury, hypoxia, or inflammation is involved in massive loss of transplanted cells.[18] On the other hand, ROS also act as regulatory signaling molecules, playing

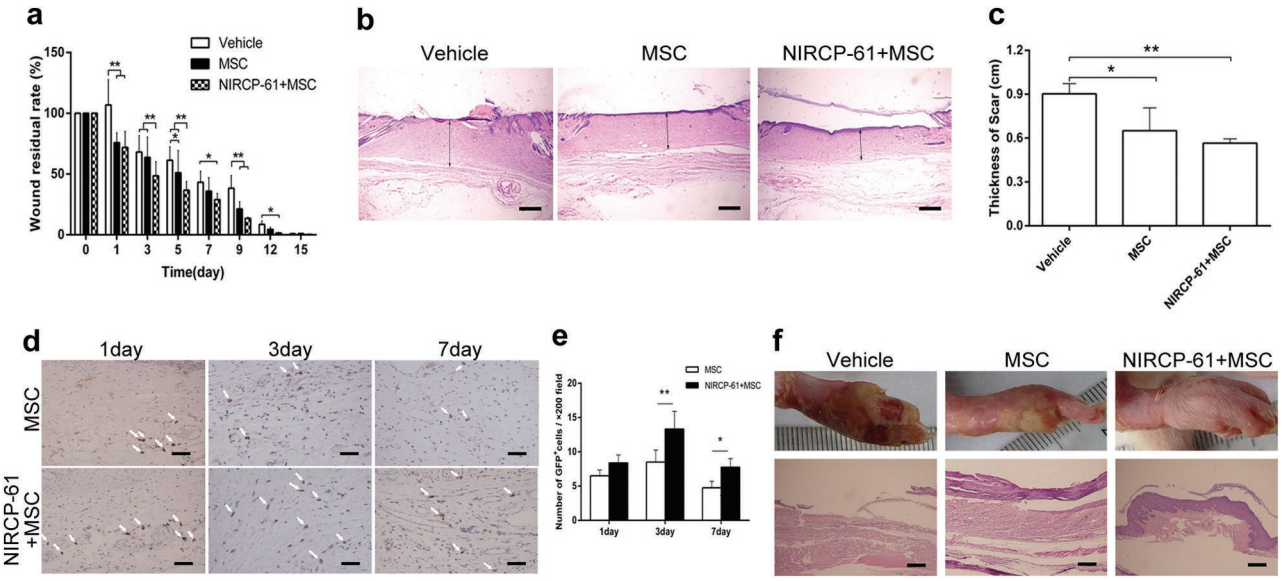

Figure 6. NIRCP-61 enhances MSCs survival in impaired tissues and accelerates wound healing. a) Wound residual area was measured every other day until cured to evaluate wound healing. Wound healing was faster in the MSCs transplanted groups, as compared to the vehicle group. NIRCP-61 further accelerates wound healing, especially at days 3 and 5 (*, $P < 0.05$; **, $P < 0.01$; $n = 6$). b) Representative images of scar thickness (H&E). c) Quantification of scar thickness. MSCs transplantation significantly decreased scar thickness (*, $P < 0.05$; **, $P < 0.01$; $n = 6$). d,e) Representative images and quantification of surviving eGFP$^+$hUCMSCs in impaired tissues (white arrows) at 1, 3, and 7 d posttransplantation (*, $P < 0.05$; **, $P < 0.01$; $n = 3$). f) Representative images of hind limb and subcutaneous tissue of rats 2 weeks after MSCs transplantation. MSCs transplantation, especially transplanting NIRCP-61-preconditioned MSCs, decreased massive IR exposure-induced cutaneous ulceration and edema, and increased restoration of dermal cells. Bars represent 500 µm (b,f) and 100 µm (d).

important physiological roles in cells at low concentrations.[19] Under normal conditions, intracellular ROS is balanced from the cell by elaborate cellular antioxidant mechanisms and is kept in check. As mitochondria are the major organelle correlate with production[20] and elimination[21] of endogenous ROS, more recently, a feasible way for regulation of mitochondria to supply cytoprotection against oxidative damage is emerging.[22] Over the past few years, mitochondria-targeted bioactive molecules were administered and used to decrease mitochondrial oxidative damage and improve cell survival and achieved some successes.[23] Under consideration of the feature of mitochondria accumulation, we developed a class of heptamethine cyanine dyes through the modification of *N*-alkyl side chains around heptamethine core in the attempt to get an ideal agent which would enhance the physiological functions of mitochondria and successfully developed NIRCP-61 as a new derivative which stimulates mitochondrial biogenesis and directly promotes antioxidative defense mechanisms. These beneficial effects are associated with endogenous cytoprotection induced by elevated intracellular ROS which activates the Nrf2 and PI3K/Akt pathways,[24] accelerating the dissociation of Nrf2 from Keap1 and induces Nrf2-targeted antioxidant gene expression.[25] In short, NIRCP-61 activates Nrf2 and PI3K/Akt pathways, which is important for promoting antioxidation and for protection against cell death (**Figure 7**).

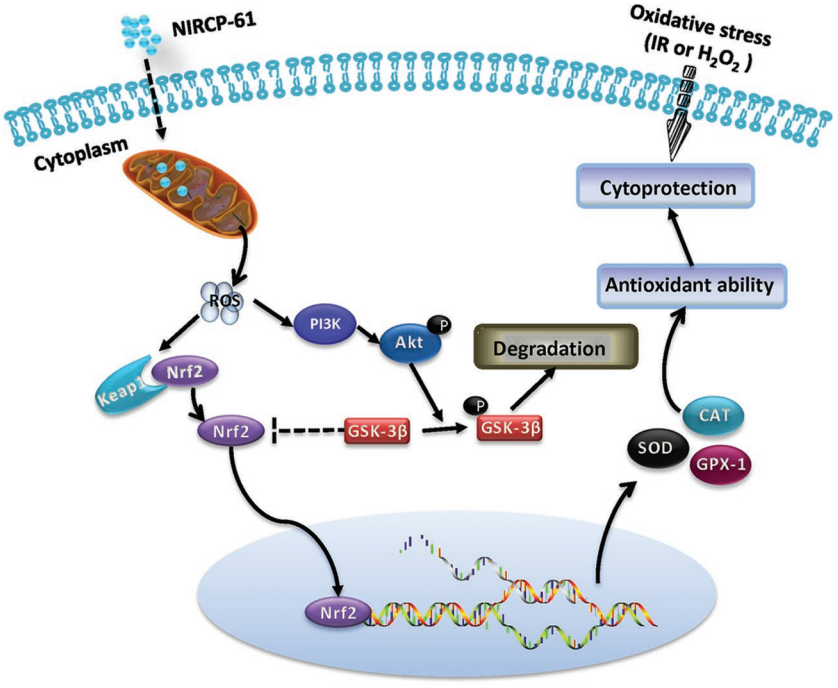

Figure 7. Proposed scheme for the mechanisms of NIRCP-61 mediated MSCs survival against oxidative stress. NIRCP-61 slightly elevates intracellular ROS level of MSCs, which accelerates Nrf2 aggregation in cytoplasm via activating Nrf2 and PI3K/Akt pathways. Increased Nrf2 nucleolus translocation elicits robust antioxidants, such as SOD, GPX-1, and CAT, and then enhances cell survival against oxidative stress and subsequently improves cell therapeutic potential.

Adv. Funct. Mater. **2016**,
DOI: 10.1002/adfm.201600996

Compared to previous mitochondria-targeted antioxidants, NIRCP-61 represents a super candidate for cytotherapy due to the property of cell labeling, because a deliberate monitoring of cell fate after transplantation would be very helpful for successfully implementing cell therapies. Therefore, NIRCP-61 may present a practicable implication in the development of mitochondria-targeted strategy for cell therapeutics.

4. Conclusion

In conclusion, we have developed a promising fluorescent agent for both cell tracking and cytoprotection with significantly increased therapeutic potential for tissue repair/regeneration in multiple animal models. The cytoprotective effect of NIRCP-61 is realized by inducing cell redox regulation, which delicately modulates the Nrf2 and PI3K/Akt signaling pathways, thereby revealing a promising strategy to enhance stem cell function to achieve improved therapeutic effects. Moreover, different from present membrane dyes or other sophisticated strategies to enhance cell viability, this newly developed agent provides a biocompatible and readily manipulated way to meet the demands of current cytotherapy. To our knowledge, this is the first agent that simultaneously facilitates NIR cell tracking and cytoprotection, which may offers a new approach to improve cell transplantation in potential clinical applications.

5. Experimental Section

Isolation and Culture of MSCs: mBMMSCs, rDMSCs, hUCMSCs, and hDMSCs were isolated and cultured as previously described.[26] eGFP$^+$mBMMSCs were isolated from eGFP transgenic mice. eGFP$^+$hUCMSCs and eGFP$^+$hDMSCs were transfected by lentiviral vectors containing small hairpin RNA-encoding sequences for eGFP (Obio Technology).

Cell Preconditioning with NIRCP-61: hUCMSCs and hDMSCs were used to optimize preconditioning condition. MSCs were preconditioned with NIRCP-61 at various incubation times and concentrations at 37 °C in the dark. After removing free dyes, cells were imaged using a Leica fluorescent microscope equipped with 633 and 700–800 nm (excitation/emission) filters. The mean fluorescent intensity of the MSCs was assessed using the Leica LAS AF Lite software. MSCs were preconditioned with 20×10^{-6} M NIRCP-61 for 30 min in other experiments, except when specifically stated otherwise.

Differentiation Assays: MSCs were seeded at 4×10^4 cells cm^{-2}; the medium was replaced every 2 d. When cells reached a 100% confluency or postconfluency, adipogenic differentiation was induced with adipogenic differentiation medium (Cyagen Biosciences). After 4 weeks of differentiation, lipid accumulation was visualized and quantified by staining with Oil Red O as described in the reagent manual. For osteogenic differentiation, MSCs were induced with osteogenic differentiation medium (Cyagen Biosciences). After 3 weeks of differentiation, cells were fixed and stained with alizarin red to visualize and quantify calcium deposits as described in the reagent manual.

Confocal Imaging: NIRCP-61-labeled hUCMSCs were costained with rhodamine123 and Miti-Tracker Green to detect intracellular localization of NIRCP-61. Cell nuclei were stained with Hoechst 33342 (Beyotime) and imaged using a confocal microscope (Leica TCS SP5). For the coculture of labeled hUCMSCs and eGFP$^+$hDMSCs, hUCMSCs were stained with NIRCP-61 or DiI (10×10^{-6} M, 30 min); after washing thrice with PBS, cells were cocultured with an equal quantity of eGFP$^+$hDMSCs for 24 and 48 h. After costaining with Hoechst 33342, cells were imaged using a confocal microscope.

Growth Curve Assay: MSCs were seeded in 96-well plates (2×10^3 cells well^{-1}), preconditioned with NIRCP-61, and cultured in 100 µL fresh medium after removing free dyes. The medium was replaced every 2 d. Cell proliferation was daily assessed for 7 d by adding 10 µL Cell Counting Kit-8 (CCK-8, Dojindo) reagents into each well; the plate was incubated for 2 h. Absorbance at 450 nm was measured using a microplate reader (Thermo Scientific).

Cell Viability Assay: Cells were seeded in 96-well plates (1×10^4 cells well^{-1}), preconditioned with various NIRCP-61 concentrations, and cultured in 100 µL fresh complete medium for 48 h. After treatment with 400×10^{-6} M H_2O_2 for 12 h, cell viability was assessed using the CCK-8 assay.

Clonogenic Survival Assay: MSCs were preconditioned with NIRCP-61 before treatment with IR. After IR (0–9 Gy), MSCs were reseeded in six-well plates (1×10^3 cells well^{-1}) and cultured for up to 14 d until colonies were clearly visible. Colonies were fixed with 4% paraformaldehyde, stained with 0.5% crystal violet, and colonies with >50 cells were counted. Plating efficacy and surviving fraction were calculated as previously described.[27] All colony images are representative of one of the three independent experiments.

Flow Cytometry Analysis of Apoptosis and ROS: Apoptosis was detected using annexin-V (BD Biosciences) as described in operating manual. NIRCP-61-preconditioned MSCs were treated with 400×10^{-6} M H_2O_2 for 12 h, then harvested, washed twice with cold PBS, resuspended in binding buffer, and incubated with annexin-V and PI (Sigma-Aldrich) for 15 min at room temperature in the dark. After incubation, cells were analyzed using flow cytometry. The fluorescent dyes H_2DCF-DA (Sigma-Aldrich) and MitoSOX Red (Molecular Probes) were used to measure the intracellular ROS and mitochondrial superoxide levels, respectively, as previously described.[28] MSCs were incubated with 5×10^{-6} M H_2DCF-DA or MitoSOX Red for 20 min at 37 °C; oxidation of H_2DCF-DA and MitoSOX Red was detected using flow cytometry.

Immunofluorescence Staining: MSCs were cultured on glass coverslips and preconditioned with NIRCP-61. After removing free dyes, cells were cultured for 3 d prior to IR (5 Gy). Then, the cells were fixed at specific time point post-IR, permeabilized with 0.1% Triton-X 100, and nuclei were stained for γ-H2AX as previously described.[29] Images were captured using a fluorescent microscope (Olympus BX51). In each experiment, 50 cells per time point were randomly counted to quantify the number of γ-H2AX per nucleus. All images shown are representative of one of the three independent experiments.

Immunohistochemistry for eGFP: Immunohistochemistry was performed as previously described.[30] Rat skin wound or heart tissues were harvested and fixed at indicated time points following eGFP$^+$hUCMSCs transplantation. Then, paraffin-embedded sections were incubated with primary rabbit anti-eGFP (1:200; Beyotime) and were detected in 3,3′-diaminobenzidine. Slides were costained with hematoxylin.

Histological Examination: Rat skin and heart tissues were fixed, embedded in paraffin, cut in 3 µm sections, and stained with H&E. Masson's trichrome staining was used to detect fibrosis in heart sections. Fibrosis percentage was calculated using the Image J software (imagej.nih.gov/ij/).

Western Blot Analysis: Proteins were separated using sodium dodecyl sulfate polyacrylamide gels, transferred to polyvinylidene difluoride membranes (Millipore), and probed with the following primary antibodies: γ-H2AX, GPX-1, GSK-3β, *p*-GSK-3β, Akt, *p*-Akt (Cell Signaling Technology), SOD1, SOD2, CAT, Nrf2, *p*-Nrf2 (Abcam), β-actin, and glyceraldehyde-3-phosphate dehydrogenase (GAPDH, Beyotime). Horseradish peroxidase-conjugated secondary antibodies (Beyotime) were applied for 2 h at room temperature. The band intensities were visualized and determined using an enhanced chemiluminescence detection system (Bio-Rad Laboratories).

Comet Assay: An alkaline comet assay was performed to assess DNA damage according to the instructions provided by the manufacturer (Comet Assay kit; Trevigen). MSCs were harvested at indicated

time points post-IR (5 Gy), resuspended in PBS, mixed with molten LMAgarose at a ratio of 1:10 (v/v), and then 50 µL agarose cells^{-1} were spread on comet slides. The slides were kept flat at 4 °C in the dark for 40 min and immersed in 4 °C lysis solution for 1 h and neutral electrophoresis buffer for 30 min. The slides were placed in an electrophoresis slide tray and voltage was applied at 1 V cm^{-1} for 45 min at 4 °C. The slides were gently immersed in DNA precipitation solution and 70% ethanol for 30 min at room temperature, stained with ethidium bromide for 5 min in the dark, and viewed using a fluorescent microscope. Quantitative analysis of at least 50 randomly selected cells per sample were analyzed using the Casplab software (casplab.com/).

Small Interfering RNA-Mediated Knockdown of Nrf2 Expression: Cells cultured in Opti-MEM Reduced Serum Media (Invitrogen) were transfected with 50×10^{-9} M Nrf2 human siRNA (Shanghai GenePharma Co., Ltd.) or negative control siRNA with Lipofectamine 2000 (Invitrogen) according to the manufacturer's instructions. Fresh culture medium was added to the cultures 6 h posttransfection. Cell transfection for other experiments was performed 2 d before use.

Animals: Sprague-Dawley (SD) rats, C57BL mice, and transgenic eGFP mice were purchased from the Laboratory Animal Center of the Third Military Medical University. Mice were executed a dorsal wound of ≈1 cm^2 after IR (5 Gy) and 2×10^6 NIRCP-61-preconditioned eGFP$^+$mBMMSCs or NIRCP-61-preconditioned eGFP$^+$mBMMSCs lysates in 200 µL PBS were injected intravenously. Animals were anesthetized and whole-body NIR fluorescence imaging was performed at time points of 10 min, 1, 3, and 7 d postinjection, respectively. After imaging, mice were sacrificed, real-time intraoperative images of animals with opening abdominal walls and thoracic cavity and ex vivo images of organs were measured. Histological analysis was performed to confirm the fluorescence detected was derived from injected eGFP$^+$mBMMSCs. To evaluate the therapeutic effects of MSCs transplantation, combined irradiation (5 Gy) and dorsal wound (1 cm^2) SD rats (3 week old) were randomly divided in the following three groups: vehicle group, MSCs group and NIRCP-61+MSCs group. Then, PBS and 2×10^6 eGFP$^+$hUCMSCs with or without NIRCP-61 preconditioning suspended in 200 µL PBS were transplanted by intravenous injection. At days 1, 3, and 7, three rats in each MSCs transplanted group were sacrificed to detect cell survival. After the wounds had healed, all rats were sacrificed. To explore the therapeutic effects of MSCs transplantation on high-dose IR, rat posterior limbs were exposed to 40 Gy IR, and 200 µL PBS or 2×10^6 hUCMSCs with or without NIRCP-61 preconditioning suspended in 200 µL PBS were infused in rats. To establish rat MI model, the left anterior descending coronary artery was permanently ligated. Male SD rats (8 week old) were randomly separated into four groups and underwent sham or MI surgery. PBS, eGFP$^+$hUCMSCs, and NIRCP-61-preconditioned eGFP$^+$hUCMSCs (1×10^5 cells in 50 µL PBS) were immediately and respectively injected at five sites in the anterior and posterior infarct border zones of the ischemic myocardium. All protocols and animal study procedures were approved by the Ethics Committee and were performed according to the Animal Care and Use Committee Guidelines of the Third Military Medical University.

Statistical Analysis: All data are presented as means ± standard deviations. Statistical analyses were applied using the Student's *t*-test and one-way analysis of variance to determine statistical significance ($P < 0.05$).

Supporting Information

Supporting Information is available from the Wiley Online Library or from the author.

Acknowledgements

X.W. and Z.C. contributed equally to this work. This work was supported by State Key Basic Research Development Program (2012CB518103), National Key Research and Development Program (2016YFC1000805), Natural Science Foundation Programs (81372727), University Innovation Team Building Program of Chongqing (CXTDG201602020), and Program of New Century Excellent Talents in University from Ministry of Education (NCET-11-0869).

Received: February 24, 2016
Revised: August 23, 2016
Published online:

[1] a) M. F. Pittenger, A. M. Mackay, S. C. Beck, R. K. Jaiswal, R. Douglas, J. D. Mosca, M. A. Moorman, D. W. Simonetti, S. Craig, D. R. Marshak, *Science* **1999**, *284*, 143; b) J. M. Gimble, A. J. Katz, B. A. Bunnell, *Circ. Res.* **2007**, *100*, 1249.

[2] a) J. A. Horton, K. E. Hudak, E. J. Chung, A. O. White, B. T. Scroggins, J. F. Burkeen, D. E. Citrin, *Stem Cells* **2013**, *31*, 2231; b) C. Rosen, E. Shezen, A. Aronovich, Y. Z. Klionsky, Y. Yaakov, M. Assayag, I. E. Biton, O. Tal, G. Shakhar, H. Ben-Hur, D. Shneider, Z. Vaknin, O. Sadan, S. Evron, E. Freud, D. Shoseyov, M. Wilschanski, N. Berkman, W. E. Fibbe, D. Hagin, C. Hillel-Karniel, I. M. Krentsis, E. Bachar-Lustig, Y. Reisner, *Nat. Med.* **2015**, *21*, 869; c) L. Hu, H. Cheng, Y. Gao, M. Shi, Y. Liu, Z. Hu, J. Xu, L. Qiu, W. Yuan, A. Y. Leung, Y. G. Yang, T. Cheng, *Blood* **2014**, *124*, e45; d) W. E. Wang, D. Yang, L. Li, W. Wang, Y. Peng, C. Chen, P. Chen, X. Xia, H. Wang, J. Jiang, Q. Liao, Y. Li, G. Xie, H. Huang, Y. Guo, L. Ye, D. D. Duan, X. Chen, S. R. Houser, C. Zeng, *Circ. Res.* **2013**, *113*, 288; e) J. Atkinson, A. A. Kapralov, N. Yanamala, Y. Y. Tyurina, A. A. Amoscato, L. Pearce, J. Peterson, Z. Huang, J. Jiang, A. K. Samhan-Arias, A. Maeda, W. Feng, K. Wasserloos, N. A. Belikova, V. A. Tyurin, H. Wang, J. Fletcher, Y. Wang, Vlasova II, J. Klein-Seetharaman, D. A. Stoyanovsky, H. Bayir, B. R. Pitt, M. W. Epperly, J. S. Greenberger, V. E. Kagan, *Nat. Commun.* **2011**, *2*, 497.

[3] E. J. Sutton, T. D. Henning, B. J. Pichler, C. Bremer, H. E. Daldrup-Link, *Eur. Radiol.* **2008**, *18*, 2021.

[4] X. Y. Wang, S. Ju, C. Li, X. G. Peng, A. F. Chen, H. Mao, G. J. Teng, *PLoS one* **2012**, *7*, e50575.

[5] a) S. E. Boddington, T. D. Henning, P. Jha, C. R. Schlieve, L. Mandrussow, D. DeNardo, H. S. Bernstein, C. Ritner, D. Golovko, Y. Lu, S. J. Zhao, H. E. Daldrup-Link, *Cell Transplant.* **2010**, *19*, 55; b) S. H. Kim, G. Park, H. Hyun, J. H. Lee, Y. Ashitate, J. Choi, G. H. Hong, E. A. Owens, M. Henary, H. S. Choi, *Biomed. Mater.* **2013**, *8*, 014110.

[6] F. Lassailly, E. Griessinger, D. Bonnet, *Blood* **2010**, *115*, 5347.

[7] S. Luo, X. Tan, Q. Qi, Q. Guo, X. Ran, L. Zhang, E. Zhang, Y. Liang, L. Weng, H. Zheng, T. Cheng, Y. Su, C. Shi, *Biomaterials* **2013**, *34*, 2244.

[8] a) S. Luo, X. Tan, S. Fang, Y. Wang, T. Liu, X. Wang, Y. Yuan, H. Sun, Q. Qi, C. Shi, *Adv. Funct. Mater.* **2016**, *26*, 2826; b) X. Tan, S. Luo, D. Wang, Y. Su, T. Cheng, C. Shi, *Biomaterials* **2012**, *33*, 2230; c) Y. Wang, T. Liu, E. Zhang, S. Luo, X. Tan, C. Shi, *Biomaterials* **2014**, *35*, 4116; d) T. Liu, S. Luo, Y. Wang, X. Tan, Q. Qi, C. Shi, *Drug Des., Dev. Ther.* **2014**, *8*, 1287.

[9] C. Zhang, X. Tan, L. Tan, T. Liu, D. Liu, L. Zhang, S. Fan, Y. Su, T. Cheng, Y. Zhou, C. Shi, *Cell Transplant.* **2011**, *20*, 741.

[10] Q. Guo, S. Luo, Q. Qi, C. Shi, *J. Innovative Opt. Health Sci.* **2013**, *06*, 1350003.

[11] S. Y. Lim, K. H. Hong, D. I. Kim, H. Kwon, H. J. Kim, *J. Am. Chem. Soc.* **2014**, *136*, 7018.

[12] B. Cai, X. Li, Y. Wang, Y. Liu, F. Yang, H. Chen, K. Yin, X. Tan, J. Zhu, Z. Pan, B. Wang, Y. Lu, *PloS One* **2013**, *8*, e63561.

[13] a) K. D. Pendergrass, A. V. Boopathy, G. Seshadri, K. Maiellaro-Rafferty, P. L. Che, M. E. Brown, M. E. Davis, *Stem*

Cells Dev. **2013**, *22*, 2414; b) Y. Zhao, C. Kong, X. Chen, Z. Wang, Z. Wan, L. Jia, Q. Liu, Y. Wang, W. Li, J. Cui, F. Han, L. Cai, *Mol. Cell. Endocrinol.* **2015**, *422*, 203.

[14] L. Madhavan, *Biochem. Soc. Trans.* **2015**, *43*, 627.

[15] S. Chowdhry, Y. Zhang, M. McMahon, C. Sutherland, A. Cuadrado, J. D. Hayes, *Oncogene* **2013**, *32*, 3765.

[16] a) J. M. Gimble, A. J. Katz, B. A. Bunnell, *Circ. Res.* **2007**, *100*, 1249; b) F. Ogura, S. Wakao, Y. Kuroda, K. Tsuchiyama, M. Bagheri, S. Heneidi, G. Chazenbalk, S. Aiba, M. Dezawa, *Stem Cells Dev.* **2014**, *23*, 717; c) X. Pei, J. Xi, X. Yan, W. Yue, J. Zhou, *Burns Trauma* **2013**, *1*, 13.

[17] a) P. K. Nguyen, J. Riegler, J. C. Wu, *Cell Stem Cell* **2014**, *14*, 431; b) S. Brown, V. Greco, *Cell Stem Cell* **2014**, *15*, 683; c) G. Chen, F. Tian, C. Li, Y. Zhang, Z. Weng, Y. Zhang, R. Peng, Q. Wang, *Biomaterials* **2015**, *53*, 265.

[18] a) E. T. Chouchani, V. R. Pell, E. Gaude, D. Aksentijevic, S. Y. Sundier, E. L. Robb, A. Logan, S. M. Nadtochiy, E. N. Ord, A. C. Smith, F. Eyassu, R. Shirley, C. H. Hu, A. J. Dare, A. M. James, S. Rogatti, R. C. Hartley, S. Eaton, A. S. Costa, P. S. Brookes, S. M. Davidson, M. R. Duchen, K. Saeb-Parsy, M. J. Shattock, A. J. Robinson, L. M. Work, C. Frezza, T. Krieg, M. P. Murphy, *Nature* **2014**, *515*, 431; b) C. R. Mantel, H. A. O'Leary, B. R. Chitteti, X. Huang, S. Cooper, G. Hangoc, N. Brustovetsky, E. F. Srour, M. R. Lee, S. Messina-Graham, D. M. Haas, N. Falah, R. Kapur, L. M. Pelus, N. Bardeesy, J. Fitamant, M. Ivan, K. S. Kim, H. E. Broxmeyer, *Cell* **2015**, *161*, 1553; c) I. Ohsawa, M. Ishikawa, K. Takahashi, M. Watanabe, K. Nishimaki, K. Yamagata, K. Katsura, Y. Katayama, S. Asoh, S. Ohta, *Nat. Med.* **2007**, *13*, 688.

[19] C. L. Bigarella, R. Liang, S. Ghaffari, *Development* **2014**, *141*, 4206.

[20] A. J. Kowaltowski, N. C. de Souza-Pinto, R. F. Castilho, A. E. Vercesi, *Free Radical Biol. Med.* **2009**, *47*, 333.

[21] A. Nickel, M. Kohlhaas, C. Maack, *J. Mol. Cell. Cardiol.* **2014**, *73*, 26.

[22] a) P. Venditti, L. Di Stefano, S. Di Meo, *Mitochondrion* **2013**, *13*, 71; b) A. Wanet, T. Arnould, M. Najimi, P. Renard, *Stem Cells Dev.* **2015**, *24*, 1957.

[23] a) W. Li, K. Jiang, W. Wei, Y. Shi, S. Ding, *Cell Res.* **2013**, *23*, 81; b) W. Li, K. Li, W. Wei, S. Ding, *Cell Stem Cell* **2013**, *13*, 270.

[24] G. Dai, S. Vaughn, Y. Zhang, E. T. Wang, G. Garcia-Cardena, M. A. Gimbrone Jr., *Circ. Res.* **2007**, *101*, 723.

[25] a) B. Chen, Y. Lu, Y. Chen, J. Cheng, *J. Endocrinol.* **2015**, *225*, R83; b) C. Zhu, S. Wang, B. Wang, F. Du, C. Hu, H. Li, Y. Feng, R. Zhu, M. Mo, Y. Cao, A. Li, X. Yu, *Neuroscience* **2015**, *304*, 328.

[26] a) H. Zhu, Z. K. Guo, X. X. Jiang, H. Li, X. Y. Wang, H. Y. Yao, Y. Zhang, N. Mao, *Nat. Protoc.* **2010**, *5*, 550; b) T. K. Chatzistamatiou, A. C. Papassavas, E. Michalopoulos, C. Gamaloutsos, P. Mallis, I. Gontika, E. Panagouli, S. L. Koussoulakos, C. Stavropoulos-Giokas, *Transfusion* **2014**, *54*, 3108; c) C. M. Chinnici, G. Amico, M. Monti, S. Motta, R. Casalone, S. L. Petri, M. Spada, B. Gridelli, P. G. Conaldi, *Cell Transplant.* **2014**, *23*, 1169.

[27] N. A. Franken, H. M. Rodermond, J. Stap, J. Haveman, C. van Bree, *Nat. Protoc.* **2006**, *1*, 2315.

[28] a) H. Song, M. J. Cha, B. W. Song, I. K. Kim, W. Chang, S. Lim, E. J. Choi, O. Ham, S. Y. Lee, N. Chung, Y. Jang, K. C. Hwang, *Stem Cells* **2010**, *28*, 555; b) R. Quintana-Cabrera, S. Fernandez-Fernandez, V. Bobo-Jimenez, J. Escobar, J. Sastre, A. Almeida, J. P. Bolanos, *Nat. Commun.* **2012**, *3*, 718.

[29] T. Sugrue, J. A. Brown, N. F. Lowndes, R. Ceredig, *Stem Cells* **2013**, *31*, 137.

[30] Z. Chen, T. Dai, X. Chen, L. Tan, C. Shi, *Stem Cell Res. Ther.* **2015**, *6*, 85.